magnetochemistry

MDPI

Article

Dye-Sensitized Molecular Charge Transfer Complexes: Magnetic and Conduction Properties in the Photoexcited States of Ni(dmit)$_2$ Salts Containing Photosensitive Dyes

Ryoma Yamamoto [1], Takashi Yamamoto [1], Keishi Ohara [1] and Toshio Naito [1,2,*]

[1] Graduate School of Science and Engineering, Ehime University, 2-5, Bunkyo-cho, Matsuyama 790-8577, Japan; c851018x@mails.cc.ehime-u.ac.jp (R.Y.); yamataka@ehime-u.ac.jp (T.Y.); ohara.keishi.mg@ehime-u.ac.jp (K.O.)

[2] Division of Material Science, Advanced Research Support Center (ADRES), Ehime University, 2-5, Bunkyo-cho, Matsuyama 790-8577, Japan

* Correspondence: tnaito@ehime-u.ac.jp; Tel.: +81-(0)89-927-9604

Academic Editor: Manuel Almeida
Received: 3 March 2017; Accepted: 12 May 2017; Published: 19 May 2017

Abstract: Photosensitive dyes often induce charge transfer (CT) between adjacent chemical species and themselves under irradiation of appropriate wavelengths. Because of the reversibility and selectivity of such CT, it is considered to be interesting to utilize such dyes as optically controllable trigger components for conduction and magnetism in the photoexcited states of organic materials. Based on this idea, such a type of new salts, i.e., γ- and δ-DiCC[Ni(dmit)$_2$] in addition to DiCC$_2$[Ni(dmit)$_2$]$_3$ have been prepared, characterized and their physical and structural properties have been examined both under dark and irradiated conditions (dmit^{2-} = 1,3-dithiole-2-thione-4,5-dithiolate, DiCC$^+$ = 3,3′-Dihexyloxacarbocyanine monocation). Among them, under UV (254–450 nm) irradiation, δ-DiCC[Ni(dmit)$_2$] exhibited photoconductivity being six times as high as its dark conductivity at room temperature. The electron spin resonance (ESR) spectra have demonstrated that there are photoexcited spins on both DiCC and [Ni(dmit)$_2$] species as a result of the CT transition between them, serving as localized spins (DiCC) and carriers ([Ni(dmit)$_2$]), respectively. The results obtained in this work have indicated that the strategy mentioned above is effective in developing organic photoresponsive semiconductors with paramagnetism.

Keywords: Ni(II)-dithiolene complex; cyanine dye; charge transfer complex; photoconduction; molecular crystal

1. Introduction

Some kind of aromatic amines and bipyridyl derivatives have attracted attention in various research fields for a long time as photosensitive dyes, which exhibit strong reducing or oxidizing abilities under irradiation [1–8]. Accordingly, they induce charge transfer (CT) between adjacent chemical species and the dyes in the photoexcited states in both solution and solid. This property often triggers various series of redox-type photochemical reactions. Some of them were originally synthesized as photosensitizers for color photographic films, and are now utilized for simplified model systems of photosynthesis [6], dye sensitized solar cells [7], and photocatalysts for clean energy [8].

Different but also interesting utilization of them includes combining them with molecular building blocks for conduction and magnetism [9–33]. Irradiation of light with appropriate wavelengths would bring about CT transition to produce unpaired electrons/holes on both of the dyes and the building blocks in a transient way. As long as the irradiation continues, the excitation and relaxation happen

one after another in a continual, rapid and repetitive manner, which practically retains the conduction and magnetism during irradiation. This would enable optical/remote control of appearance and disappearance of conduction and magnetism in an immediate and reversible way.

In fact, such examples have been recently reported [10–12,16]. It has been demonstrated that metallic and paramagnetic properties can be realized in some CT complexes containing bipyridyl derivatives and π-acceptor molecules under UV irradiation. They have mixed-stacking structures with almost fully ionized cations and anions, and are practically diamagnetic insulators under dark conditions. These physical properties are natural judging from their crystal structures and formal charges. Since this structure–property correlation is convincing and generally the case, these kinds of solids has been avoided in the field of molecular conductors. This assumption is true under dark conditions. However, in the photoexcited states, there is metallic conduction coexisting with semiconducting contribution from thermal carriers even in such solids. In addition, one requires low-conducting materials under the dark condition for high photoresponse. Thus, the finding above suggests that there should be a different guideline for development of conducting and magnetic materials under irradiation from the established one for thermodynamically stable metals.

Based on this idea, various kinds of organic CT salts have been prepared. Particular attention has been paid to well-known photosensitizers such as methyl viologen (Scheme 1) and cyanine dyes. By utilizing them as counter cations, a series of $[Ni(dmit)_2]$ radical anion salts ($dmit^{2-}$ = 1,3-dithiole-2-thione-4,5-dithiolate; Scheme 1) has been found to form a group of interesting candidates. Among them, there are four kinds of $DiCC^+$ salts ($DiCC^+$ = 3,3′-Dihexyloxacarbocyanine monocation; Scheme 1) with the same stoichiometry but with different crystal structures; α-, β-, γ-, δ-$DiCC[Ni(dmit)_2]$. The α-salt is known [13], yet because of its poor crystal quality and because it is seldom obtained, details still remain elusive. The structural and physical properties of β-salt under dark conditions have been recently reported by our group [13], while the two salts (γ- and δ-salts) are newly obtained. In addition, single crystals with a different stoichiometry, $DiCC_2[Ni(dmit)_2]_3$ (2:3-salt), have been also newly obtained. In this article, the physical and structural properties of the new salts (γ-, δ- and 2:3-salts) are presented, and are compared with each other in order to discuss the factors and conditions for efficient photoresponsive conducting and magnetic properties.

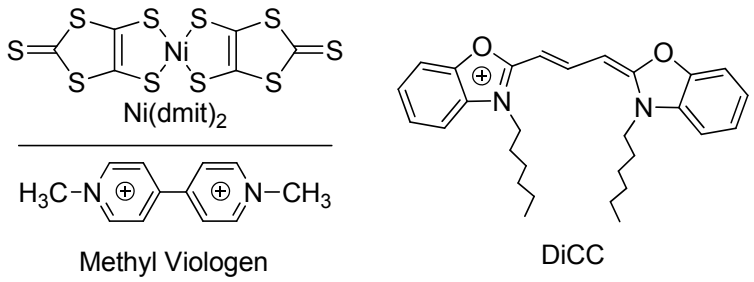

Scheme 1. Chemical structures of compounds.

2. Results

2.1. Crystal Structures, Similarities and Differences among the DiCC Salts

The crystal structures of γ-, δ- and 2:3-salts are shown in Figures 1–3. The crystallographic data are summarized in Table 1. As for the molecular structures, all of the interatomic distances and angles were normal for both anions and cations, and their arrangements were also standard for these types of compounds. In order to make it clear what the important features are for high photoresponse in conduction and magnetism, we should now pay more attention to comparison of their structures than details of each structure. The single crystals of these salts were all (elongated) black platelets. Considering the color of the starting materials (dark green and reddish orange for $[Ni(dmit)_2]^-$ and

DiCC$^+$, respectively) of their synthesis, the black color suggests some intermolecular interaction involving CT.

Table 1. Summary of crystallographic data.

Salt	γ	δ	2:3
Cation:Anion	1:1	1:1	2:3
Formula	$C_{35}H_{37}N_2NiO_2S_{10}$	$C_{35}H_{37}N_2NiO_2S_{10}$	$C_{76}H_{74}N_4Ni_3O_4S_{30}$
M (g mol^{-1})	896.99	896.99	2245.26
Temperature (K)	296	296	296
Crystal system	Triclinic	Monoclinic	Triclinic
Space Group	$P\bar{1}$(#2)	$P2_1/n$ (#14)	$P\bar{1}$(#2)
a (Å)	8.36861(17)	10.8163(5)	7.7933(4)
b (Å)	13.7285(3)	30.5876(12)	12.7677(6)
c (Å)	18.2519(4)	12.4468(5)	25.2676(10)
α (°)	79.6321(11)	–	76.977(2)
β (°)	80.7564(11)	95.6803(17)	88.978(3)
γ (°)	83.0074(11)	–	76.505(3)
V (Å^3)	2026.57(7)	4097.7(3)	2380.29(19)
Z	2	4	1
D_{calc} (g cm^{-3})	1.470	1.454	1.566
μ (Cu $K\alpha$) (cm^{-1})	57.784	57.155	72.288
CCDC deposit #	1526722	1526720	1526726
Reflection/Parameter	15.82	16.49	15.87
Max peak (e$^-$/Å^3)	0.66	0.63	0.89
Min peak (e$^-$/Å^3)	−0.48	−0.71	−0.60
R_1, wR_2	0.0563 [1], 0.1950 [2]	0.0731 [1], 0.2486 [2]	0.0733 [1], 0.2194 [2]
GOF	1.124	1.038	0.929
Max Shift/Error	0.007	0.000	0.066

[1] $I > 2.00\sigma(I)$. [2] All reflections.

The three salts were basically comprised of mixed-stacking structures or alternate arrangement of cations and anions like ionic crystals. This structural common feature suggests that Coulombic attraction between anions and cations should overwhelm the π–π interaction between ions with the same charge in these salts. Closer examination clarified that both cations and anions were almost completely planar except for the hexyl groups of the DiCC cations, and neighboring molecules were parallel and/or close to each other, suggesting π–π interaction between them. This feature manifested itself in 2:3-salt, where there were two types of stacking columns, i.e., anion-only columns in addition to anion-cation mixed columns. Thus, it appears that overall molecular arrangement in these salts should be governed by the Coulombic and π–π interactions. It is the unique feature common to these salts that the crystals most developed along the cation–anion interactions, in contrast to other Ni(dmit)$_2$ semiconducting salts. It is often the case with the Ni(dmit)$_2$ salts that their crystals mostly develop in parallel with the Ni(dmit)$_2$ sheets or columns in which the Ni(dmit)$_2$ anions closely interact with each other.

The differences in the conformation of hexyl groups in the cations affected the resultant molecular arrangements only in a quantitative way such as intermolecular distances. The following subsections briefly describe selected details of the structure of each salt, which will provide us information necessary for understanding the physical properties discussed below.

2.1.1. γ-Salt

The single crystals were elongated hexagonal platelets and most developed along the *a*-axis. The unit cell consisted of an asymmetric unit containing a cation and an anion (Figure 1a), and possessed a mixed-stacking structure along the *a*-axis.

The two hexyl groups of the cation extended approximately in the plane of the π-conjugated part of the molecule. In other words, the entire cation was nearly planar (Figure 1b).

For conduction and magnetism, the interaction between the $Ni(dmit)_2$ anions is important. In γ-salt, the anions formed a loosely-assembled sheet in the *bc*-plane (Figure 1b,c), and there were some short distances between them shorter than or comparable to the van der Waals distance between two sulfur atoms (3.70 Å; Figure 1d).

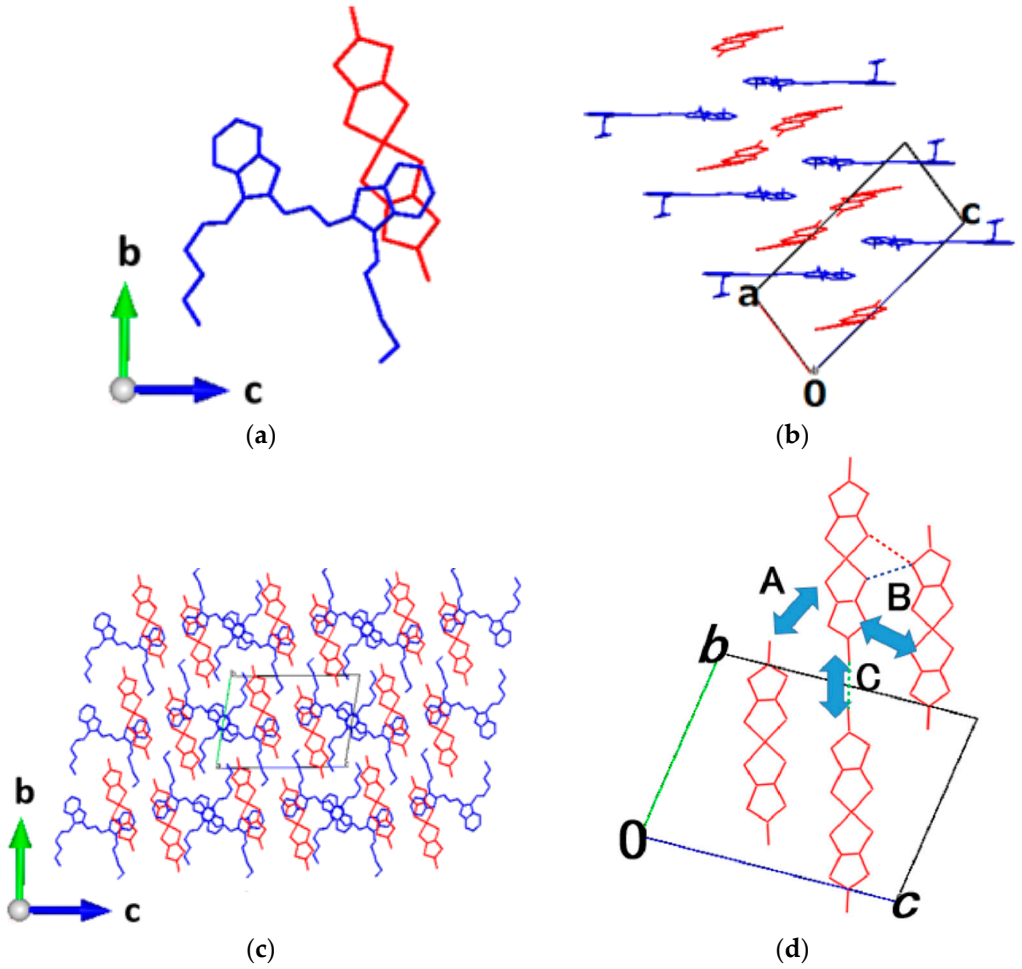

Figure 1. Crystal structure of γ-DiCC[$Ni(dmit)_2$] (DiCC = 3,3′-Dihexyloxacarbocyanine monocation). Red; $Ni(dmit)_2$ anon, blue; DiCC cation, hydrogen atoms are omitted for clarity: (**a**) asymmetric unit; (**b**) view down along *b*-axis; (**c**) view down along *a*-axis; (**d**) interaction between anions in the *bc*-plane. In (**d**), the shortest sulfur–sulfur distances between the two anions designated by broken lines are 3.280(2) (green, in relation C), 3.572(2) (blue, B), 3.705(2) Å (red, B), respectively.

2.1.2. δ-Salt

The single crystals were elongated thick platelets and most developed along the *a*-axis. The unit cell of δ-salt consisted of an asymmetric unit containing a cation and an anion, and can be regarded as a mixed-stacking structure along the *a*-axis.

The direction in which the two hexyl groups extended (Figure 2a) was different from that in γ-salt (Figure 1a). The two hexyl groups of the cation extended almost vertically to the plane of the π-conjugated part of the molecule, and they extended in a parallel way to each other but in an opposite way to those of the neighboring cation (Figure 2b).

Still, in γ-salt, the neighboring mixed-stacking columns are solid-crossing to each other (Figure 2c,d), and, at the crossing points, there were short distances between the adjacent anions in different columns shorter than or comparable to the van der Waals distance between two sulfur atoms.

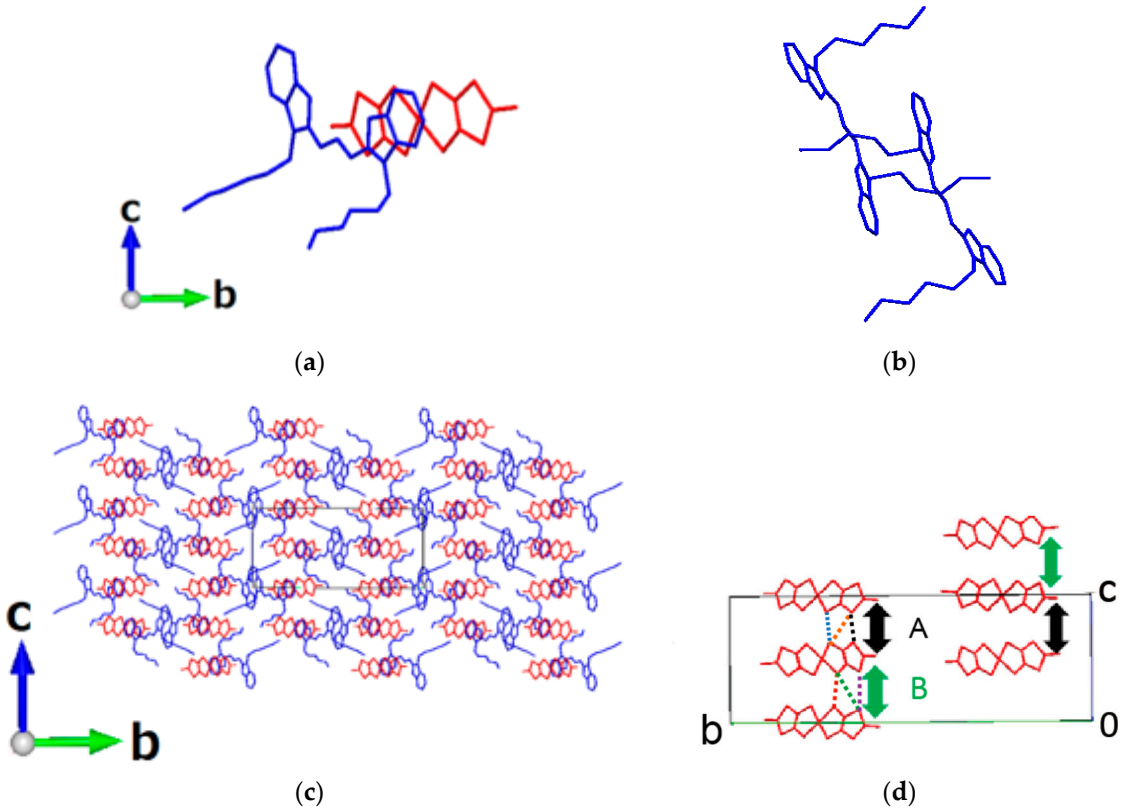

Figure 2. Crystal structure of δ-DiCC[Ni(dmit)$_2$]. Red; Ni(dmit)$_2$ anon, blue; DiCC cation, hydrogen atoms are omitted for clarity: (**a**) asymmetric unit; (**b**) neighboring cation arrangement; (**c**) view down along *a*-axis; (**d**) interaction between anions in the *bc*-plane. In (**d**), the sulfur–sulfur distances between the two anions designated by broken lines are 3.747(2) (blue), 3.519(2) (orange) and 3.656(2) Å (black) in the intermolecular relation A and 5.312(2) (red), 4.474(2) (green) and 3.819(2) Å (violet) in the relation B, respectively.

2.1.3. 2:3-Salt

The single crystals were elongated thick platelets (parallelepipeds) and most developed along the [210]-direction, which was nearly parallel (~15°) with the *a*-axis. The unit cell of 2:3-salt consisted of an asymmetric unit containing a whole cation and one and a half of anions (Figure 3a). There were two kinds of stacking columns along the *a*-axis: cation–anion mixed-stacking columns and anion-only columns. Accordingly, the structure of 2:3-salt possessed both features of insulating and conducting molecular CT complexes; the former was common to the structures of the 1:1-salts (β- [13], γ-, and δ-) and those often observed in the fully ionized (ionic) molecular CT complexes. The latter structural feature is considered to originate from two factors; one is the non-integer charges on cations and anions due to the small amount of CT between cations and anions in the ground state, and the other is the molecular shapes and sizes to allow them to share the similar intermolecular distances between the two different types of columns (anion-only, and anion–cation mixed types).

The direction in which the two hexyl groups extended was different either from that in γ-salt or that in δ-salt. The two hexyl groups of the cation extended as if they surround the anion-only columns (Figure 3b). There were some short distances (<3.70 Å) between sulfur atoms on neighboring

anions, which could form conduction pathways (Figure 3c). Considering the sulfur–sulfur interatomic contacts, the most conductive direction should be in the *a*-axis.

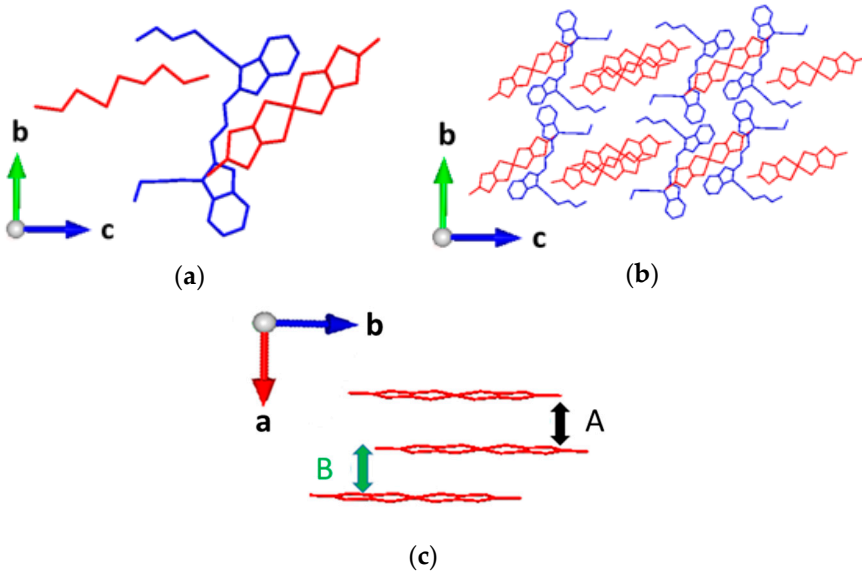

Figure 3. Crystal structure of $DiCC_2[Ni(dmit)_2]_3$. Red; $Ni(dmit)_2$ anon, blue; DiCC cation, hydrogen atoms are omitted for clarity: (**a**) asymmetric unit containing one and a half of the anions and a whole cation; (**b**) view down along *a*-axis; (**c**) interaction between anions in stacking columns along the *a*-axis. In (**c**), the shortest sulfur–sulfur distances between the two anions designated as A and B are 3.792(3) and 3.688(3) Å, respectively.

2.2. Electrical Behavior

As the conducting and magnetic properties of these salts are expected to be governed by the $Ni(dmit)_2$ anions, resistivity should be measured in the direction where the anions aggregate themselves to form conduction pathways of columns or sheets. However, in these salts, the dimensions of the single crystals in such directions were too small to carry out electrical measurements, suggesting that the interactions between the anions are not so large compared with other intermolecular interactions. Based on the structural analyses above, the common feature of these three salts is that cations and anions alternate with each other along the longest axis of each crystal. In these types of crystals, the electrical resistivity along the longest axis is considered to be dominated by the hopping of carriers between cations and anions. Additionally, the photoresponse should be largest when the CT bands between cations and anions are excited, since the CT transitions produce holes and electrons, corresponding to net carrier doping to both species. Such CT requires cation–anion π–π interactions, which can be estimated by resistivity measurements in the penetrating direction through cations and anions. Therefore, the electrical resistivity measurements were carried out on the single crystals of these salts along the longest axes concerning both dark conductivity and photoresponse.

The γ-salt was highly insulating with room temperature conductivity of 7.9×10^{-9} Scm^{-1} (// *a*-axis) both under dark and irradiated conditions irrespective of incident wavelength in UV-Vis region (Figure 4a). The photoresponse is corroborated by its diffuse reflectance spectra (Figure A1 in Appendix), where no CT bands were observed in 200–2500 nm. This result is also consistent with the electron spin resonance (ESR) spectra under irradiation, where no response (spectral change) was observed either.

The δ-salt exhibited 100 times as high dark conductivity as the remaining salts, 8.6×10^{-7} Scm^{-1} (// *a*-axis) at room temperature, and even higher conductivity under UV-irradiation by six times, 5.2×10^{-6} Scm^{-1} (// *a*-axis) at room temperature, compared with its dark conductivity (Figure 4b).

The 2:3-salt was also highly insulating with room temperature conductivity of 8.3×10^{-9} Scm^{-1} (// *a*-axis) both under dark and irradiated conditions irrespective of incident wavelength in UV-Vis region (Figure 4c). Such negligible photoresponse in conduction is consistent with the diffuse reflectance spectra of UV-Vis-NIR (Figure A1 in Appendix), where CT bands were hardly observed like the case of γ-salt.

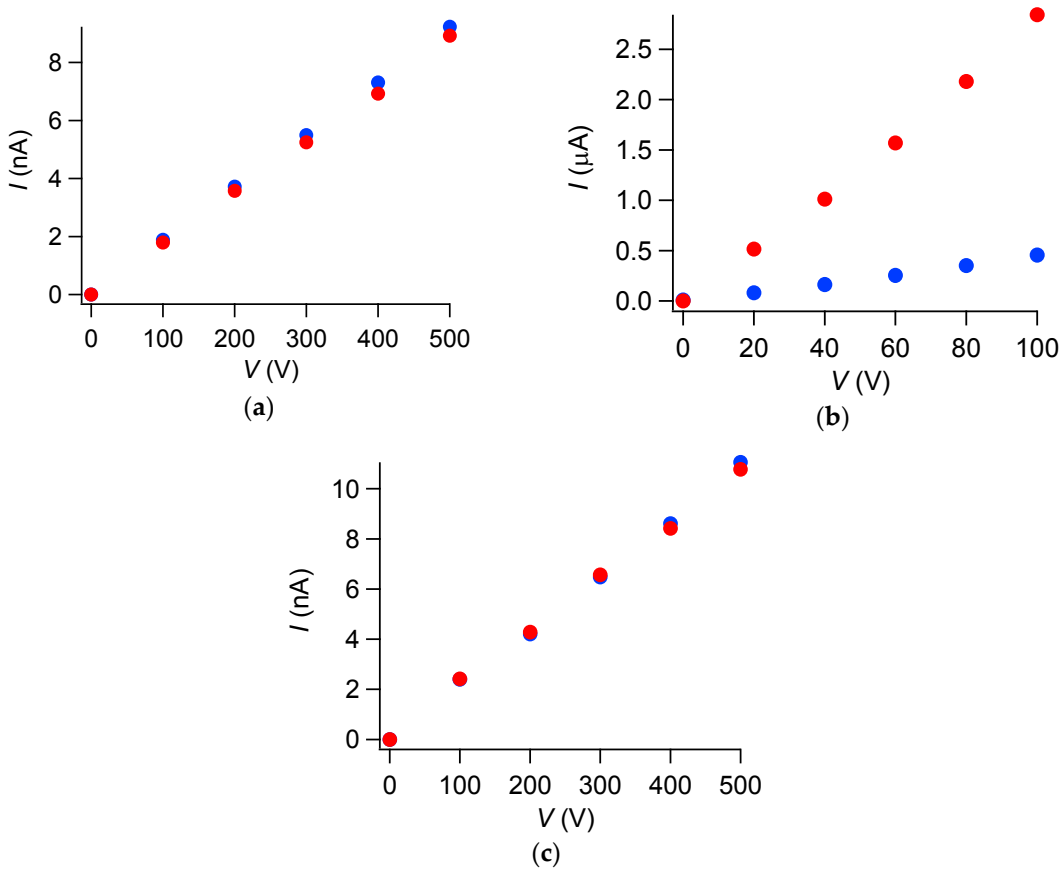

Figure 4. Observed current under dark and UV-irradiated conditions of γ-, δ- and 2:3-salts. Red; under UV-irradiation (254–450 nm), blue; under dark condition: (**a**) γ-salt; (**b**) δ-salt; (**c**) 2:3-salt.

2.3. Electron Spin Resonance (ESR)

The ESR spectra under dark and irradiated conditions for γ- and δ-salts are shown in Figures 5 and 6, together with simulated spectra considering hyperfine interactions with nuclear spins, linewidths, and *g*-values in an anisotropic way. As a result, the obtained parameters are rather isotropic or two-dimensional, as is often the case with π-spins. The best fit parameters corresponding to the simulated spectra are summarized in Tables A1–A3 in the Appendix. The irradiated conditions were identical with those in the electrical resistivity measurements. The ESR was not measured for 2:3-salt because it was highly insulating and did not exhibit any photoresponse in conduction.

Based on the ESR of β-salt in our previous work [13] as well as the spectral simulation in this work, all of the spectra consisted of two sets of peaks originating from the spins on the cations (~325–330 mT) and those on the anions (~315–320 mT), respectively. However, their relative intensities, overall lineshapes, and photoresponses depended on the salts. Some of the peaks could not be reproduced in a quantitative way, i.e., in all of the peak positions, the lineshapes, the linewidths and the intensities. Still, overall spectral features are well reproduced by the simulation for all the three salts, enabling semi-quantitative discussion for us.

The spectra of γ-salt did not change at all between dark and irradiated conditions (Figure 5), which agreed with the photoresponse in electrical behavior. This is consistent with the crystal structure.

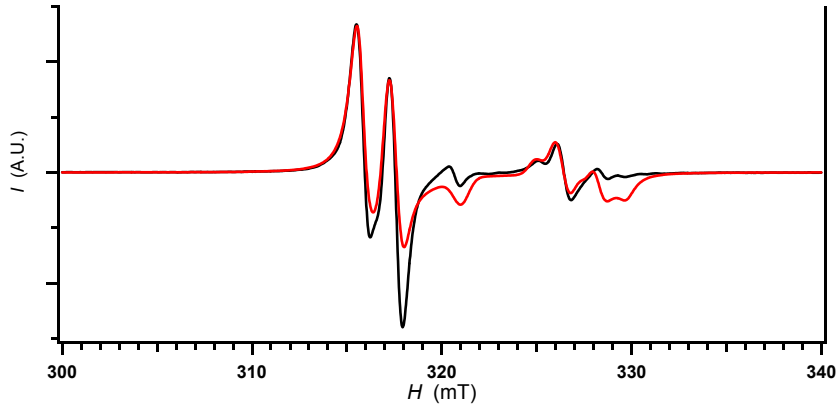

Figure 5. Electron spin resonance (ESR) spectra of γ-salt measured under dark and irradiated (254–450 nm) conditions. Black; observed spectra, red; simulated spectra. The observed spectra were completely identical and overlapped with each other under dark and irradiated conditions.

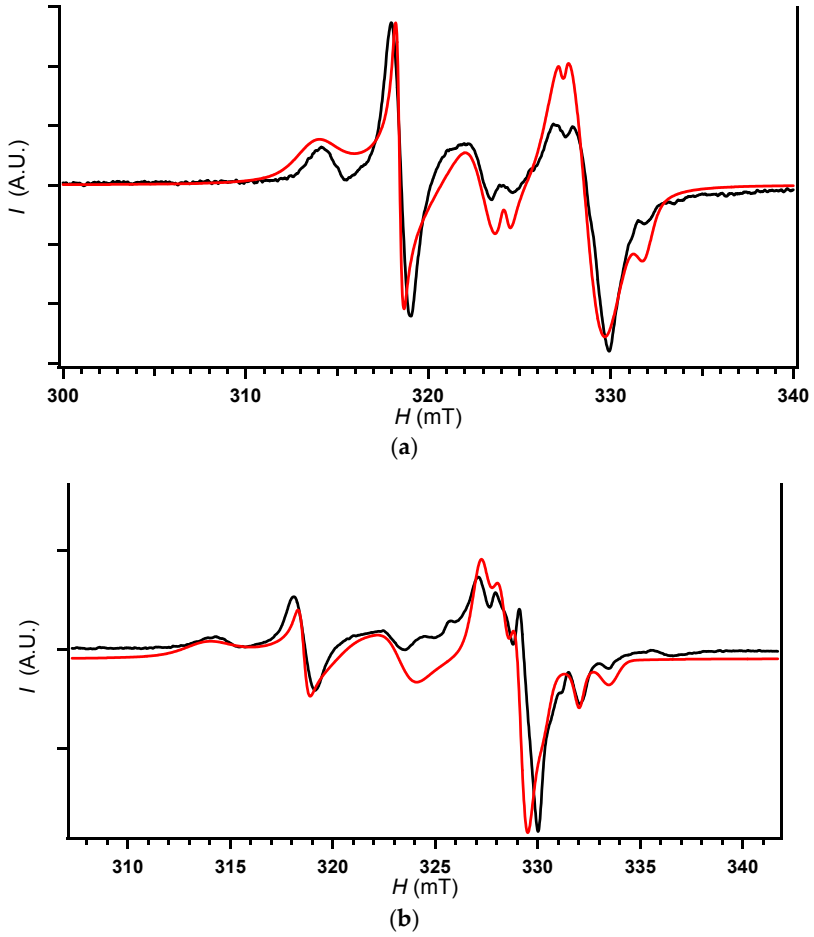

Figure 6. ESR spectra of δ-salt measured under dark and irradiated (254–450 nm) conditions. Black; observed, red; simulated spectra: (**a**) spectrum under dark condition and its simulated spectrum; (**b**) spectrum under irradiated condition and its simulated spectrum.

The spectra of δ-salt under UV-irradiation were clearly different from its spectra under dark conditions (Figure 6). Under dark conditions, the total intensity of peaks due to the spins on the anions (anions' peaks) was comparable to or slightly larger than that due to the spins on the cations (cations' peaks). In contrast, under UV-irradiation, the relative intensity of the cations' peaks reversibly

increased to become much more intense than those of anions' peaks, almost retaining the lineshapes and *g*-values. This implies that CT transition occurs between cations and anions under UV-irradiation. As the CT transitions between two different components in solids produce net photocarriers and photoexcited spins at the same time [10–12,16], the observed photoresponse in ESR spectra accounts for the observed photoresponse in electrical behavior mentioned above. The *g*-values of a part of the spins on the N atoms (#3 (N) in the dark conditon in Table A2 were markedly enhanced compared with those of isolated spins on the bipyridine derivatives (g ~2.00 for N atoms), indicating strong interaction with the spins having larger *g*-values such as those in heavy atoms and transition metals, i.e., indicating strong interaction between cations and anions. This is consistent with the crystal structure. By comparison between Tables A2 and A3, the simulation of the ESR spectra indicates that the spin densities on the cations relative to the anions increases in the photoexcited state than that in the dark state. This indicates that the photoexcitation corresponds to the CT from the anions to the cations producing localized spins on the cations and doping holes in the anions' bands at the same time.

3. Discussion

3.1. Structure–Property Relations

The obtained results thus far are summarized in Table 2 for comparison. The CT interactions between cations and anions and those between anions are important for production of charge carriers and forming conduction pathways, respectively. However, if they are too strong between a particular pair of molecules, other interactions would inevitably become small. Accordingly, an occurrence of a strong interaction will lead to strong dimerization as is the case in γ- and 2:3-salts. Such a situation corresponds to uneven potential with deep valleys and high barriers for carriers to go through, which is evidently unfavorable to electrical conduction and favorable for localization of unpaired electrons in deep valleys.

As regards carriers, because the photoexcitation can produce/increase them to some extent, the lack of carriers in the ground state does not matter so seriously compared to dark conductivity. In principle, a small (large) cation–anion CT interaction generally involves a large (small) amount of charge transfer between them with a small (large) transition probability. In addition, the actual conduction depends also on the produced carriers' mobility and the mean free path in the excited states/bands as well as those in the originally fully-occupied states/bands. The mobility and relaxation times depend on the characteristics of the bands, and is practically independent of the number of carriers produced unless their densities are high. Therefore, the interrelation between photoresponse and the strength of cation–anion interaction is complicated. The cation–anion CT interaction is necessary for high photoresponse ($\sigma_{photo}/\sigma_{dark}$), yet interaction that is too strong often leads to unfavorable situations for photoconduction, as is the case in the dark conduction.

Table 2. Comparison of properties of DiCC salts (DiCC = 3,3′-Dihexyloxacarbocyanine monocation).

Salts	Dark Conductivity σ_{dark} (Scm^{-1})	Photoconductivity [1] σ_{photo} (Scm^{-1})	$\sigma_{photo}/\sigma_{dark}$	Anion–Anion Interaction [2]	Cation–Anion Interaction [2]
γ	7.9×10^{-9}	7.9×10^{-9}	1	Uneven	Weak
δ	8.6×10^{-7}	5.2×10^{-6}	6	Very weak	Moderate
2:3	8.3×10^{-9}	8.3×10^{-9}	1	Strongly dimerized columns	Strong

[1] Here, "photoconductivity" means the conductivity under irradiation, and the observed values may include contributions of dark conductivity and thermal carriers. [2] Estimated by the structural features.

Thus far, we have not explicitly discussed the possible structural differences between dark and photoexcited states. We have not obtained any data indicating or excluding such a structural change on photoexcitation in these salts, and nothing can be said until some evidence will be obtained in future work.

As regards the relaxation times of photoexcited carriers and localized spins, the ESR spectra of the "photosilent" salts (γ- and 2:3-salts) left us an important message. Whether they exhibit photoresponse in conduction or not, there should be photoexcited spins/carriers in them during the ESR measurements under photoirradiation as long as they absorb the light. However, irradiation did not change the ESR spectra of γ-salt or conduction behavior of γ- and 2:3-salts at all. This can be explained by considering the relaxation times. In the ESR spectra under UV-irradiation, there are at least two kinds of relaxation times, that of UV-excitation (τ_{UV}) and that of ESR, i.e., microwave-excitation (τ_{ESR}). For the observation of ESR on the photoexcited unpaired electrons, the condition $\tau_{UV} >> \tau_{ESR}$ is required. In addition, if τ_{ESR} in these salts are too short or too long compared with 10^{-10} s, they are not observed in ESR spectra measured using X-band microwaves (9–10 GHz). General substances do not satisfy these requirements, and do not exhibit photoresponses in ESR. Similarly, the increase in conductivity would not be observed under irradiation, when τ_{UV} is far shorter than the time scale of resistivity measurement (~1–10 ms), even if there are a sufficient number of photocarriers with sufficient mobilities. This situation is clearly different from dark conductivity, where carriers can be discussed based on a single kind of relaxation time characteristic of their mean free path. Since all of these salts absorb UV-Vis-NIR light (~10^{15} Hz), τ_{UV} should be on the order of 10^{-15} s, and succeeding processes are considered to differ from each other to result in different relaxation times of photoexcited carriers on the anions and localized spins on the cations. Based on the discussion thus far, the overall relaxation time of photoexcited spins on the cations and anions is unusually prolonged to produce the observed photoresponse in ESR and conduction. Such prolonged relaxation times have been observed only in the CT complexes containing bipyridine derivatives with apparently mixed-stacking structures [10–12]. The mechanism can be related to the characteristic or advantage in this kind of molecular CT complexes such as CT interactions with photosensitive dyes, which would stabilize the photoexcited states. It can be also the key feature for mechanism that they exhibit rather high conduction along the mixed-stacking direction. The detailed experiments are now under way to clarify the mechanism.

3.2. Material Design for and beyond Photoconductors

The $Ni(dmit)_2$ salts with photosensitizer cations were obtained and one of them exhibited semiconducting behavior with a moderately high ratio between photoconduction relative to its dark conduction and unusually long relaxation times of photoexcited carriers and localized spins. This photoexcited behavior is considered to be closely related to the interaction between $DiCC^+$ and $[Ni(dmit)_2]^-$ species, which produces carriers and localized spins under UV-irradiation. This structural feature originates from the intermediate molecular packing between ionic and molecular crystal structures with retaining anion–anion molecular orbital overlaps narrowly.

The molecular design and combination strategy here is different from that for molecular metals and superconductors. In the design of highly conducting materials, smaller counter ions are favorable for close packing and self-aggregation of $[Ni(dmit)_2]^-$. Additionally, the partial oxidation of $[Ni(dmit)_2]^-$ is required for production of carriers. However, highly conducting materials generally do not exhibit high photoconductivity; semiconducting or insulating behavior is required under the dark condition. Here in this work, a rather bulky π-conjugated counter species ($DiCC^+$) and fully ionized $[Ni(dmit)_2]^-$ were utilized, which produced a semiconductor with low conductivity.

For efficient photoresponsive conductors and magnets, the relaxation times of photoexcited electrons are one of the most important factors. The long relaxation times observed here have never been reported in known materials for photoelectric conversion, whether they are organic or inorganic, and thus can be a suitable or superior new material for solar cells/photovoltaics, for example. Accordingly, δ-salt proves that the combination of dye sensitizers and π-conjugated radical anions/cations is a promising strategy to photoresponsive semiconductors and paramagnets as next-generation molecular functional materials.

4. Materials and Methods

4.1. Sample Preparation

3,3′-Dihexyloxacarbocyanine iodide (DiCC·I) (Sigma-Aldrich, St. Louis, MO, USA, 98%) and acetonitrile (Wako Pure Chemicals, Osaka, Japan, Super Dehydrated Grade) were purchased and used as received. [n-$(C_4H_9)_4$N][Ni(dmit)$_2$] (abbreviated as TBA[Ni]) was synthesized by following the reported procedure [34]. The single crystals of all kinds of salts DiCC$_n$[Ni(dmit)$_2$]$_m$ {(n, m) = (1,2) or (2,3)} were obtained from the salt metathesis of DiCC·I and $(C_4H_9)_4$N[Ni(dmit)$_2$] in CH_3CN. The polycrystalline solid of DiCC·I (3 mg) and TBA[Ni] (3 mg) were separately dissolved in 10 mL of acetonitrile and filtered. The former solution was added to the latter solution, and the resulting mixed solution stood still being loosely sealed with a sheet of plastic (polyvinylidene chloride) film at room temperature (RT) under dark conditions to allow gradual evaporation of the solvent until precipitation of the crystals were observed. This procedure yielded γ-, δ- and 2:3-salts as a mixture after a week. Attempts to find synthetic conditions for them in a selective way remain unsuccessful. The single crystals were filtered and washed thoroughly with acetonitrile and acetone, and dried in vacuo. The obtained crystals were identified based on the X-ray oscillation photographs (cell parameters), and subjected to electrical resistivity and ESR measurements.

4.2. X-ray Structural Analysis

The data collection was carried out at 296 K for γ-, δ-, and 2:3-salts using R-AXIS RAPID (Rigaku, Tokyo, Japan). Radiation used was graphite monochromated Cu Kα (λ = 1.54187 Å) for all the salts. The structural analysis was carried out using CrystalStructure 4.1 (Rigaku, Tokyo, Japan). The details are summarized in Supplementary Materials. Crystallographic data have been deposited with Cambridge Crystallographic Data Centre (CCDC): the deposition numbers are summarized in Table 1.

4.3. Physical Measurements

4.3.1. Electrical Resistivity Measurements

The single crystals were freshly prepared and checked in advance by X-ray oscillation photographs for the quality, morphology (to confirm the direction of the crystallographic axes for identifying most conductive direction) and phase (α-, β-, γ-, δ- or 2:3-salts). Both ends of the needle or platelet crystal (~0.5–1 mm) were freshly cut immediately before every measurement, and gold wires were attached upon the fresh cross sections.

As the electrical resistivity of these compounds were found to be generally high (bulk resistance $R > 10^7$ ohm) based on the preliminary measurements, the resistivity measurements were carried out by a direct-current two-probe method. All of the measurements were carried out at 296 K under ambient pressure, and the temperature raise due to Joule heating effects was checked by time-resolved resistivity measurements with the time resolution of 18 ms by the same equipment [13] and on the spot, and temperature and/or resistivity data were taken at the equilibrium/constant states. Their resistivity was too high to measure at low temperature whether under dark or irradiated conditions, and thus the temperature dependence was not measured. A constant voltage (Table 3) was applied and the resultant current was measured. The voltage was varied in a range to confirm the linearity between the voltage and the current to exclude any artifact. The constant voltage was applied along the largest dimensions (longest axes, edges or diagonals) of the crystals. The equipment was homemade cryostat consisting of a picoammeter/voltage source (Keithley 6487, Tektronix, Inc., Beaverton, OR, USA) or a sourcemeter (Keithley 2400, Tektronix, Inc., Beaverton, OR, USA), a digital temperature controller (Model 331, Lake Shore Cryotronics, Inc., Westerville, OH, USA), and a rotary/diffusion packaged pumping system (DS-A412N, Diavac Limited, Yachiyo, Japan). Gold paste (No. 8560, Tokuriki Honten Co., Ltd., Tokyo, Japan) and gold wires (25 μm in diameter; Nilaco 171086, The Nilaco Corporation,

Tokyo, Japan) were used as the electrical contacts. All the measurements of dark conductivity were carried out in a double-shielded copper sample room with a helium atmosphere (~2–5 Pa at RT) under complete darkness. After dark conductivity, the photoconductivity was measured on the same sample in an open atmosphere. The light was guided through an optical fiber to be normal on the sample surface and the distance between the end of the fiber and sample was 1 cm. The light source used was Hg/Xe-Lamp (200 W, Supercure-203S, San-Ei Electric, Osaka, Japan) equipped with adjustable power gain and filters. The irradiation conditions are summarized in Table 4.

Table 3. Conditions in electrical resistivity measurements. [1]

Salt	Direction	Start (V)	End (V)	Interval (V)
γ	// *a*-axis	100	500	100
δ	// *a*-axis	20	100	20
2:3	~// *a*-axis [2]	100	500	100

[1] Common to dark and photoconductivity measurements. The current and voltage were applied and measured in the direction indicated. In order to check linearity between voltage and current, which is required for electrical resistivity measurements, the measurement was carried out by applying six different voltages in series by increasing the voltage from the value of Start [V] to that of End [V] with the interval [V] indicated in the table. [2] The exact direction was the [210]-direction, which was nearly parallel (~15°) with the *a*-axis.

Table 4. Irradiation conditions in photoconductivity measurements. [1]

Salt	Wavelength Range (1) (nm)	Intensity (1) (Wcm^{-2})	Wavelength Range (2) (nm)	Intensity (2) (Wcm^{-2})
γ	254–450	6.7	254–1100	12.3
δ	254–450	6.7	NA	NA
2:3	254–450	6.7	254–1100	12.3

[1] Some samples were examined under two different irradiation conditions.

4.3.2. Electron Spin Resonance (ESR)

All of the ESR measurements were carried out using single crystals. The single crystal, which was briefly checked by X-ray oscillation photographs, was set on a piece of silicone sheet with Apiezon N grease (Apiezon, Manchester, UK). This was set on a piece of Teflon with Apiezon N in a quartz ESR tube (5 mm in diameter) with the proper alignment relative to the magnetic field, and the tube was sealed in a helium atmosphere (~10–20 kPa). The measurements were carried out using a JES-FA100 (X-band spectrometer; 9.3 GHz, JEOL Ltd., Tokyo, Japan) at a constant temperature. The temperature was controlled so as not to allow the temperature variation to exceed ±0.5 K during the field sweep. The magnetic field was corrected by a Gaussian meter (NMR Field Meter ES-FC5, JEOL Ltd., Tokyo, Japan) at the end of every measurement. The accuracy of magnetic fields was further confirmed by a single crystal of DPPH (1,1-Diphenyl-2-picrylhydrazyl; g = 2.00366 ± 0.00004) [35–37], which was used as a standard of g-values. The temperature (77 K), sweep time (30 s), modulation (100 kHz), microwave power (0.998 mW), and time constant (0.01 s) were identical for each salt and common to the measurements under dark and irradiated conditions. The time constants were varied and finally determined to be the best values considering signal:noise ratio and observation of details of the lineshapes (hyperfine structures). For every salt, the ESR measurements under dark conditions were carried out first. Then, the sample in the ESR tube was irradiated for 10 min through an optical fiber and a focusing lens in situ through an optical window of the ESR cavity. For all of the salts, the ESR spectra gradually changed during the first several minutes of irradiation. After confirming that the spectra did not change any more, the spectra were recorded under continuous irradiation by integrating the spectra by 10–20 times. The spectra simulation was carried out using Anisotropic Simulation software AniSim/FA ver. 2.2.0 (JEOL Ltd., Tokyo, Japan). In the simulation, the parameters for g-value, hyperfine coupling constants A (mT) of ^{14}N (I = 1) and ^{1}H (I = 1/2), linewidth Γ (mT), and the ratio between Lorentzian and Gaussian were considered in an anisotropic way.

4.3.3. Diffuse Reflectance Spectra

Diffuse reflectance spectra in the UV-vis-NIR (200–2500 nm) region were measured for the samples dispersed in a KBr pellet and sandwiched with a pair of quartz glasses with a U-4000 spectrophotometer (Hitachi High-Technologies Corporation, Tokyo, Japan) at RT with a resolution of 2 nm.

Supplementary Materials: The following are available online at www.mdpi.com/2312-7481/3/2/20/s1

Acknowledgments: This work was partially supported by Ehime University GP, and an Ehime University. Grant for Interdisciplinary Research.

Author Contributions: T.N. and R.Y. conceived and designed the experiments; R.Y. performed the experiments; T.N. and R.Y. analyzed the data; T.Y. and K.O. helped R.Y. in the measurements of resistivity and ESR, respectively; and T.N. wrote the paper.

Conflicts of Interest: The authors declare no conflict of interest. The founding sponsors had no role in the design of the study; in the collection, analyses, or interpretation of data; in the writing of the manuscript, and in the decision to publish the results.

Appendix A. Diffuse Reflectance Spectra

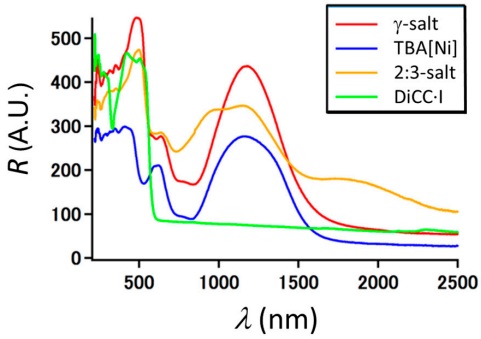

Figure A1. Diffuse reflectance spectra of γ- and 2:3-salts (powder). Spectra of [n-$(C_4H_9)_4$N][Ni(dmit)$_2$] (TBA[Ni]) and DiCC·I (both in powder) are also shown for comparison. Red; γ-salt, blue; [n-$(C_4H_9)_4$N][Ni(dmit)$_2$], yellow; 2:3-salt, green; DiCC·I.

Appendix B. Electron Spin Resonance (ESR) Spectra

Table A1. Parameters for simulated spectrum of γ-salt [a,b].

Spin # [c]	#1	#2	#3	#4
I_{rel} (%)	82.8	13.9	1.65	1.65
I	0 (^{32}S)	0 (^{32}S)	1 (^{14}N)	1 (^{14}N)
g_x	2.0855	2.0743	2.0060	2.0180
g_y	2.0855	2.0743	2.0060	2.0175
g_z	1.9970	2.0510	2.0058	2.0160
A_x (mT)	NA	NA	0.100	1.300
A_y (mT)	NA	NA	0.100	0.100
A_z (mT)	NA	NA	0.100	0.100
Γ_x (mT)	0.660	0.700	0.800	0.700
Γ_y (mT)	0.660	0.700	0.800	0.800
Γ_z (mT)	0.650	0.800	1.000	1.000
Lorentzian/Gaussian	100/0	0/100	100/0	100/0

[a] The observed spectra were completely identical and overlapped with each other under dark and irradiated conditions. Thus, the parameters shown above are common to both spectra under dark and irradiated conditions. [b] I_{rel}, I, g_i, A_i and Γ_i (i = x, y, z) designate relative intensity, nuclear spin, g-value, hyperfine coupling constant and linewidth in the i-direction, respectively. [c] Spin # designate the serial numbers of the oscillators required for the reproduction of the observed spectra. It does not mean that there are such numbers of independent spins in the sample.

Table A2. Parameters for simulated spectrum of δ-salt under dark conditions [a].

Spin # [b]	#1	#2	#3	#4
I_{rel} (%)	82.5	6.19	1.03	10.3
I	0 (^{32}S)	0 (^{32}S)	1 (^{14}N)	1 (^{14}N)
g_x	2.0980	2.0500	2.0310	2.0040
g_y	2.0680	2.0400	2.0308	2.0040
g_z	1.9843	2.0328	2.0112	2.0040
A_x (mT)	NA	NA	0.100	0.100
A_y (mT)	NA	NA	0.100	0.100
A_z (mT)	NA	NA	0.100	0.100
Γ_x (mT)	2.000	2.000	0.800	2.200
Γ_y (mT)	0.300	1.300	0.300	2.200
Γ_z (mT)	0.800	1.000	0.150	2.200
Lorentzian/Gaussian	80/20	100/0	100/0	50/50

[a] I_{rel}, I, g_i, A_i and Γ_i ($i = x, y, z$) designate relative intensity, nuclear spin, g-value, hyperfine coupling constant and linewidth in the i-direction, respectively. [b] Spin # designate the serial numbers of the oscillators required for the reproduction of the observed spectra. It does not mean that there are such numbers of independent spins in the sample.

Table A3. Parameters for simulated spectrum of δ-salt under irradiated condition [a].

Spin # [b]	#1	#2	#3	#4
I_{rel} (%)	63.8	26.6	7.98	1.60
I	0 (^{32}S)	0 (^{32}S)	1 (^{14}N)	1 (^{14}N)
g_x	2.0980	2.0500	2.0048	2.0008
g_y	2.0670	2.0370	2.0048	2.0006
g_z	1.9832	1.9745	2.0043	2.0004
A_x (mT)	NA	NA	1.000	1.200
A_y (mT)	NA	NA	1.000	0.100
A_z (mT)	NA	NA	0.100	0.100
Γ_x (mT)	2.000	2.000	0.800	0.600
Γ_y (mT)	0.400	1.300	0.800	0.600
Γ_z (mT)	0.400	0.800	0.800	0.600
Lorentzian/Gaussian	80/20	100/0	80/20	100/0

[a] I_{rel}, I, g_i, A_i and Γ_i ($i = x, y, z$) designate relative intensity, nuclear spin, g-value, hyperfine coupling constant and linewidth in the i-direction, respectively. [b] Spin # designate the serial numbers of the oscillators required for the reproduction of the observed spectra. It does not mean that there are such numbers of independent spins in the sample.

References

1. Watanabe, T.; Honda, K. Measurement of the excitation coefficient of the methyl viologen cation radical and the efficiency of its formation by semiconductor photocatalysis. *J. Phys. Chem.* **1982**, *86*, 2617–2619. [CrossRef]
2. Mohammad, M. Methyl viologen neutral MV: 1. Preparation and some properties. *J. Org. Chem.* **1987**, *52*, 2779–2782. [CrossRef]
3. Yoon, K.B.; Kochi, J.K. Direct observation of superoxide electron transfer with viologens by immobilization in zeolite. *J. Am. Chem. Soc.* **1988**, *110*, 6586–6588. [CrossRef]
4. Yoon, K.B.; Kochi, J.K. Shape-selective access to zeolite supercages. Arene charge-transfer complexes with viologens as visible probes. *J. Am. Chem. Soc.* **1989**, *111*, 1128–1130. [CrossRef]
5. Bockman, T.M.; Kochi, J.K. Isolation and oxidation-reduction of methylviologen cation radicals. Novel disproportionation in charge-transfer salts by X-ray crystallography. *J. Org. Chem.* **1990**, *55*, 4127–4135. [CrossRef]
6. Akins, D.L.; Guo, C. Photoinduced electron transfer in synthetic model systems. *Adv. Mater.* **1994**, *6*, 512–516. [CrossRef]

7. Guo, J.; Nie, J.; Lv, Z. Synthesis and properties of bipyridyl-based dye-sensitizers. *Res. Chem. Intermed.* **2013**, *39*, 4247–4257. [CrossRef]
8. Coe, B.J.; Sanchez, S. Synthesis and properties of new mononuclear Ru(II)-based photocatalysts containing 4,4′-diphenyl-2,2′-bipyridyl ligands. *Dalton Trans.* **2016**, *45*, 5210–5222. [CrossRef] [PubMed]
9. Naito, T.; Inabe, T. Molecular conductors containing photoreactive species. *J. Phys. IV* **2004**, *114*, 553–555. [CrossRef]
10. Naito, T.; Karasudani, T.; Mori, S.; Ohara, K.; Konishi, K.; Takano, T.; Takahashi, Y.; Inabe, T.; Nishihara, S.; Inoue, K. Molecular photoconductor with simultaneously photocontrollable localized spins. *J. Am. Chem. Soc.* **2012**, *134*, 18656–18666. [CrossRef] [PubMed]
11. Naito, T.; Karasudani, T.; Ohara, K.; Takano, T.; Takahashi, Y.; Inabe, T.; Furukawa, K.; Nakamura, T. Simultaneous control of carriers and localized spins with light in organic materials. *Adv. Mater.* **2012**, *24*, 6153–6157. [CrossRef] [PubMed]
12. Naito, T.; Karasudani, T.; Nagayama, N.; Ohara, K.; Konishi, K.; Mori, S.; Takano, T.; Takahashi, Y.; Inabe, T.; Kinose, S.; et al. Giant photoconductivity in NMQ[Ni(dmit)$_2$]. *Eur. J. Inorg. Chem.* **2014**, *2014*, 4000–4009. [CrossRef]
13. Saiki, T.; Mori, S.; Ohara, K.; Naito, T. Capacitor-like behavior of molecular crystal β-DiCC[Ni(dmit)$_2$]. *Chem. Lett.* **2014**, *43*, 1119–1121. [CrossRef]
14. Noma, H.; Ohara, K.; Naito, T. [Cu(dmit)$_2$]$^{2-}$ Building block for molecular conductors and magnets with photocontrollable spin distribution. *Chem. Lett.* **2014**, *43*, 1230–1232. [CrossRef]
15. Noma, H.; Ohara, K.; Naito, T. Direct control of spin distribution and anisotropy in Cu-dithiolene complex anions by light. *Inorganics* **2016**, *4*. [CrossRef]
16. Naito, T. Development of control method of conduction and magnetism in molecular crystals. *Bull. Chem. Soc. Jpn.* **2017**, *90*, 89–136. [CrossRef]
17. Kisch, H.; Fernández, A.; Wakatsuki, Y.; Yamazaki, H. Charge transfer complexes of nickel dithiolenes with methyl viologen. *Z. Naturforsch.* **1985**, *40B*, 292–297. [CrossRef]
18. Fernández, A.; Görner, H.; Kisch, H. Photoinduzierte elektronenübertragung mit metalldithiolenen. *Chem. Berichte* **1985**, *118*, 1936–1948. [CrossRef]
19. Lahner, S.; Wakatsuki, Y.; Kisch, H. Charge-transfer-komplexe von metalldithiolenen mit viologenen. *Chem. Berichte* **1987**, *120*, 1011–1016. [CrossRef]
20. Nüßlein, F.; Peter, R.; Kisch, H. Viologene als redoxaktive akzeptoren–synthese und electrische leifähigkeit. *Chem. Berichte* **1989**, *122*, 1023–1030. [CrossRef]
21. Kisch, H.; Nüsslein, F.; Zenn, I. Molekulare steuerung von festkörpereigenschaften: Die elecktrische leitfähigkeit von metal-organischen charge-transfer komplexen. *Z. Anorg. Allg. Chem.* **1991**, *600*, 67–71. [CrossRef]
22. Kisch, H.; Dümler, W.; Nüßlein, F.; Zenn, I.; Chiorboli, C.; Scandola, F.; Albrecht, W.; Meier, H. Consequences of thermal and photochemical electron transfer on solution and solid state properties of metal organic ion pairs. *Z. Phys. Chem.* **1991**, *170*, 117–127.
23. Meier, H.; Albrecht, W.; Kisch, H.; Nunn, I.; Nüsslein, F. Photoconductivity of metal dithiolate ion-pair complexes. *Synth. Met.* **1992**, *48*, 111–127. [CrossRef]
24. Kisch, H. Charge-transfer in ion pairs: Design of photoconductivity in solution and electrical dark-and photoconductivity in the solid. *Coord. Chem. Rev.* **1993**, *125*, 155–172. [CrossRef]
25. Lemke, M.; Knoch, F.; Kisch, H. Structure of the ion-pair charge-transfer complex (methylviologen)$^{2+}$[Pd(mnt)$_2$]$^{2-}$. *Acta Cryst.* **1993**, *C49*, 1630–1632. [CrossRef]
26. Nunn, I.; Eisen, B.; Benedix, R.; Kisch, H. Control of electrical conductivity by supramolecular charge-transfer interactions in (dithiolene)metalate-viologen ion pairs. *Inorg. Chem.* **1994**, *33*, 5079–5085. [CrossRef]
27. Kisch, H. Electron transfer modelling of electrical dark- and photoconductivity of redoxactive ion pairs. *Comments Inorg. Chem.* **1994**, *16*, 113–132. [CrossRef]
28. Knoch, F.; Ammon, U.; Kisch, H. Crystal structure of *N*,*N*′-dimethyl-2,2′-bipyridinium bis(*cis*-1,2-dicyanoethane-1,2-dithiolato)palatinate(II), ((CH$_3$)C$_5$NH$_4$C$_5$NH$_4$(CH$_3$))(Pt(S$_2$C$_2$(CN)$_2$)$_2$). *Z. Kristallographie* **1995**, *210*, 77–78.
29. Hofbauer, M.; Möbius, M.; Knoch, F.; Benedix, R. Ion-pair charge-transfer complexes of a dithiooxalate zinc donor component with viologens. Synthesis, structural and electronic characterization. *Inorg. Chim. Acta* **1996**, *247*, 147–154. [CrossRef]

30. Götz, B.; Knoch, F.; Kisch, H. Bis(maleonitriledithiolato)oxomolybdate(IV)-bipyridinium ion pairs. *Chem. Berichte* **1996**, *129*, 33–37. [CrossRef]
31. Kisch, H. Tailoring of solid state electrical conductivity and optical electron transfer activation of dioxygen in solution through supramolecular charge-transfer interaction in ion pairs. *Coord. Chem. Rev.* **1997**, *159*, 385–396. [CrossRef]
32. Handrosch, C.; Dinnebier, R.; Bondarenko, G.; Bothe, E.; Heinemann, F.; Kisch, H. Charge-transfer complexes of metal dithiolenes XXVI Azobipyridinium dications and radical monocations as acceptors. *Eur. J. Inorg. Chem.* **1999**, *1999*, 1259–1269. [CrossRef]
33. Kisch, H.; Eisen, B.; Dinnebier, R.; Shankland, K.; David, W.I.F.; Knoch, F. Chiral metal-dithiolene/viologen ion pairs: Synthesis and electrical conductivity. *Chem. Eur. J.* **2001**, *7*, 738–748. [CrossRef]
34. Steimecke, G.; Sieler, H.-J.; Kirmse, R.; Hoyer, E. 1,3-dithiol-2-thion-4,5-dithiolat aus schwefelkohlenstoff und alkalimetall. *Phosphorus Sulfur* **1979**, *7*, 49–55. [CrossRef]
35. Yordanov, N.D. Quantitative EPR spectrometry—"State of the art". *Appl. Magn. Reson.* **1994**, *6*, 241–257. [CrossRef]
36. Kai, A.; Miki, T. Electron spin resonance of sulfite radicals in irradiated calcite and aragonite. *Radiat. Phys. Chem.* **1992**, *40*, 469–476. [CrossRef]
37. Inokuchi, H.; Kinoshita, M. The oxygen effect on electronic properties of α,α′-diphenyl-β-picrylhydrazyl. *Bull. Chem. Soc. Jpn.* **1960**, *33*, 1627–1629. [CrossRef]